Journal of The Electrochemical Society

Translocation Behaviors of Synthetic Polyelectrolytes through Alpha-Hemolysin (α-HL) and Mycobacterium smegmatis Porin A (MspA) Nanopores

Journal of The Electrochemical Society, 2022 **169** 057510
1945-7111/2022/169(5)/057510/5/$40.00 © 2022 The Electrochemical Society ("ECS"). Published on behalf of ECS by IOP Publishing Limited

Translocation Behaviors of Synthetic Polyelectrolytes through Alpha-Hemolysin (α-HL) and Mycobacterium smegmatis Porin A (MspA) Nanopores

Xiaoqin Wang,[1] Kaden C. Stevens,[2] Jeffrey M. Ting,[2] Alexander E. Marras,[2] Gelareh Rezvan,[1] Xiaojun Wei,[1,3] Nader Taheri-Qazvini,[1,3] Matthew V. Tirrell,[2] and Chang Liu[1,3,z]

[1]*Department of Chemical Engineering, University of South Carolina, Columbia, South Carolina 29208, United States of America*
[2]*Pritzker School of Molecular Engineering, University of Chicago, Chicago, Illinois 60637, United States of America*
[3]*Biomedical Engineering Program, University of South Carolina, Columbia, South Carolina 29208, United States of America*

DNAs have been used as probes for nanopore sensing of noncharged biomacromolecules due to its negative phosphate backbone. Inspired by this, we explored the potential of diblock synthetic polyelectrolytes as more flexible and inexpensive nanopore sensing probes by investigating translocation behaviors of PEO-b-PSS and PEO-b-PVBTMA through commonly used alpha-hemolysin (α-HL) and *Mycobacterium smegmatis* porin A (MspA) nanopores. Translocation recordings in different configurations of pore orientation and testing voltage indicated efficient PEO-b-PSS translocations through α-HL and PEO-b-PVBTMA translocations through MspA. This work provides insight into synthetic polyelectrolyte-based probes to expand probe selection and flexibility for nanopore sensing.
 [DOI: 10.1149/1945-7111/ac6c55]

Manuscript submitted February 20, 2022; revised manuscript received April 19, 2022. Published May 11, 2022. *This paper is part of the JES Focus Issue on Biosensors and Nanoscale Measurements: In Honor of Nongjian Tao and Stuart Lindsay.*

Supplementary material for this article is available online

Nanopore-based sensors have attracted much attention from researchers from biomedical science, chemistry, and engineering technology. It is a highly innovative technique that analyzes single molecules at nanoscale dimensions without labels or amplification at high throughput, which is difficult to achieve in bulk systems.[1–4] Over the past decade, nanopore sensing technology based on biological and solid-state nanopores has made significant progress toward high sensitivity detection for a variety of biomolecules including amino acids, peptides, and proteins.[3,5–11] Particularly prominent is the nanopore DNA/RNA sequencing, which is of paramount importance to medicine and the life sciences have obtained great promotion.[12–15]

In typical laboratory experiments using biological nanopores, a single pore-forming protein is embedded in a phospholipid membrane and single-channel electrophysiology measurements are taken. The pore-forming protein is a hollow core passing through a mushroom-shaped protein molecule for alpha-hemolysin (α-HL).[16,17] α-HL pore protein consists of seven alpha-hemolysin subunits, they oligomerize, creating ring-shaped heptamer complexes.[18] α-HL vestibule has a positive charge and biological nanopore-based sensing allows for the detection of charged polymers, including deoxyribonucleic acid[19] and ribonucleic acid (RNA), with sub-nanometer resolution, thereby precluding the need for labels or signal amplification.[19–22] Molecular recognition between nanopore and analytes could be modulated by introducing hydrophobic, aromatic, positively, and negatively charged functional groups inside the nanopore at the sensing sites.[23] Recently, DNA was used as a probe for other uncharged biomacromolecules such as proteins and peptides, providing translocation driving force through nanopores.[3,24–26] To improve the resolution in these systems, DNA has also been conjugated to uncharged peptides.[24,27] Aerolysin Mycobacterium smegmatis porin A (MspA) is a goblet-shaped molecule that shows a negative charge in the channel constriction.[28,29] MspA has a short and narrow channel constriction that is promising for DNA sequencing because it may enable improved characterization of short segments of an ssDNA molecule that is threaded through the pore.[28] And recently MspA is widely used in other biomacromolecule analysis including peptides, DNA/RNA.[30,31]

Polycations or polyanions on polyelectrolytes dissociate in polar solvents like water, making them charged.[32] Inspired using the natural polyelectrolyte DNA as a probe for nanopore sensing, we hypothesize that synthetic polyelectrolytes might also be used as probes to enable noncharged peptides and protein to be detected by nanopore. However, DNA only has a negative charge due to the phosphate backbone, whereas synthetic polyelectrolytes could be designed with a variety of negatively or positively charged groups in a number of different configurations and architectures which could expand the versatility of translocation probes and allow for the use of different types of nanopores. Inspired by neutral polyethylene glycol (PEG) oligomers widely used for nanopore sensing,[33–35] we found a negative diblock polyelectrolytes consist of neutral polyethylene oxide (PEO) and poly(styrene sulfonate) (PSS) (PEO-b-PSS), and a positive diblock polyelectrolytes consist of PEO and poly(vinylbenzyl) trimethylammonium (PVBTMA) with great potential as polyelectrolytes probes.[36]

Inspired by the success of charged DNA-neutral peptide conjugates, we investigated the translocation behavior of charged-neutral synthetic diblock polyanions and polycations through the commonly used biological nanopores α-HL and MspA with the aim of developing a synthetic probe for detecting noncharged peptides and proteins via nanopores. These two polyelectrolytes showed different translocation behaviors in different configurations of pore orientation and applied voltage. PEO-b-PSS showed the highest rate of translocation through α-HL whereas PEO-b-PVBTMA translocation was optimized through MspA. Moreover, electrolyte concentration and pH had a significant impact on translocation frequency, which revealed how environmental factors affect the interaction between polyelectrolytes and pores. This study provides insight into the design of biosensing probes based on synthetic polyelectrolytes, which might significantly expand the probe selection within nanopore sensing and the flexibility of the selection of the corresponding pores, to facilitate accurate detection of biological macromolecules detection by nanopore technology.

Experimental

Materials.—PEO-b-PSS and PEO-b-PVBTMA were synthesized according to previous methods and provided by the Tirrell group.[36]

[z]E-mail: changliu@cec.sc.edu

MspA recombinant protein was purchased from MyBioSource (CA, USA). Potassium chloride (KCl), Tris hydrochloride (Tris-HCl), α-HL from *Staphylococcus aureus* (lyophilized powder, Protein ~60% by Lowry, ⩾10,000 units mg^{-1} protein) were purchased from Sigma-Aldrich (St. Louis, MO). All working solutions were prepared using deionized water from a Milli-Q water purification system (resistivity 18.2 MΩ cm^{-1}, 25 °C, Millipore Corporation) and were filtered with 0.02 μm filters before use.

Measurement of zeta potential.—Zeta potential of polymers was measured in solution (1 mg ml^{-1}) with a Zetasizer (Nano-ZS, Malvern Instruments) at 25 °C. HCl (0.5 M) and NaOH (0.5 M) were used to adjust the pH of the solution automatically by MPT-2 Titrator (Malvern Instruments).

Work solution preparation.—KCl (7.46 g) and Tris-HCl (0.04 g) were dissolved in 70 ml deionized water, then HCl (1 M, stock concentration) and NaOH (1 M, stock concentration) were used to adjust pH to 8.0, and at last, the solution was diluted to 100 ml to get the electrolyte solution (1 M KCl and 10 mM Tris-HCl, pH 8.0). Similarly, other electrolyte solutions with different concentrations (2 M, 3 M), and different pH (4.0, 6.0, 10.0) were prepared following this protocol.

Single-channel current detection.—The Planar Lipid Bilayer Workstation (Warner Instruments) was applied to record resistive pulse signals at room temperature (21 °C ~ 25 °C). Fabrication of α-HL and MspA nanopore devices followed a traditional protocol that has been previously reported.[28,37] A Delrin chamber (25 μm thick) with an aperture (200 μm in diameter) partition *cis* (grounded) and *trans* compartments. First, the *trans* side was precoated with 1:10 hexadecane/pentane solution (Sigma-Aldrich). Next, both compartments were added with 1 ml of KCl electrolyte solution buffered in 10 mM Tris-HCl. Then 20 μl (10 mg ml^{-1}) 1, 2 diphytanoyl-sn-glycero-3-phosphocholine (Avanti Polar Lipids) dissolved in pentane (Sigma-Aldrich) was added to the *cis* side of chambers to allow the self-assembly of lipid bilayer membrane in the aperture. After confirmation of membrane formation by membrane capacitance, the electrical potential was applied to the *trans* side through Ag/AgCl electrodes and switched between ±100 mV to ensure the stability of the membrane. At last, *trans* side voltage was held at 100 mV and a small amount (~2 μg) of α-HL or MspA protein was added to the *cis* side of the chamber to insert a single nanopore channel into the lipid bilayer membrane. After a stable α-HL or MspA single nanopore was inserted and confirmed by open-pore current, a polymer analyte was added to the *cis* compartment for detection.

Data analysis.—Resistive pulse current recordings were collected using a patch-clamp amplifier (Warner Instruments) at a holding potential of ±100 mV. After the sample was added into the *cis* chamber, magnetic stirring was applied to disperse the sample well in the electrolyte solution before signals were recorded. Each sample was measured in three fresh nanopores. The raw data were analyzed using an in-house Matlab-based algorithm to find the frequency of events, which indicted the translocation rate of polymers when they pass through nanopores. According to the open pore current of each nanopore, we set 25%~30% of the current drop as a cut-off level to analyze polymer events frequencies. Results processed by the Matlab algorithm were confirmed by manual inspection.

Results and Discussion

Nanopore working principle and α-HL and MspA single open pore.—In a typical nanopore platform detection, a single biological nanopore (e.g., α-HL) is inserted into a phosphate lipid bilayer that separates *cis* and *trans* compartments in an electrolyte solution, as shown in Fig. 1a. An external positive voltage is applied to the *trans* side of the bilayer, while the *cis* side is electrically grounded.

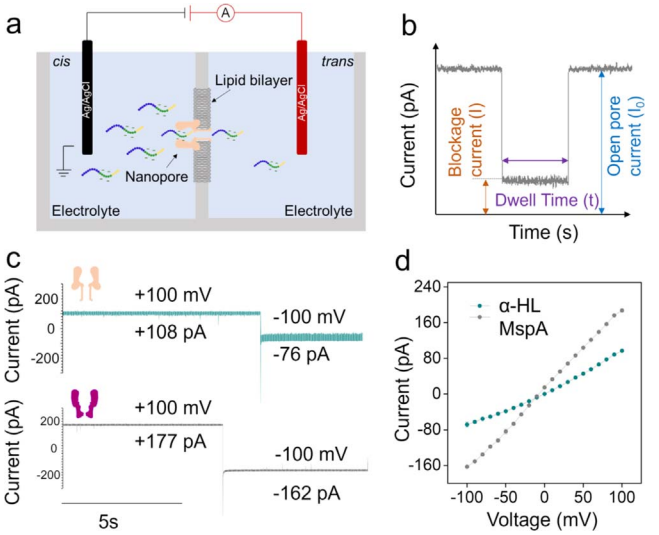

Figure 1. (a) Schematic working principal illustration of nanopore-based sensing platform; (b) Nanopore resistive pulse signal; (c) A single open pore baseline of α-HL and MspA; (d) I–V curves of single open α-HL and MspA nanopores. Data was collected in 1 M KCl,10 mM Tris-HCl buffer, pH 8.0 with applied voltage held at ±100 mV.

The analytes translocate nanopores that generate resistive pulse signals. In a resistive pulse signal (Fig. 1b), the blockage current I (i.e., residual current) indicates the capture of single molecules and their translocation through the nanopore, while the open pore current I_0 (i.e., baseline current) represents the ionic current in absence of analytes. Dwell time (i.e., duration, t) is the time difference between the start and end of an event, which indicates the effective interaction time between nanopore and a single molecule analyst.[38,39]

Figure 1c represents baseline recordings of a single open pore of α-HL and MspA. When the applied voltage was held at +100 mV, the open pore current was +108 pA for α-HL and +177 pA for MspA. When the applied voltage was held at −100 mV, the open pore current was −76 pA for α-HL and −162 pA for MspA. The open-pore currents of α-HL and MspA are asymmetric when the applied voltage flipped from positive to negative, which was caused by ionic current rectification due to the asymmetric tip geometry of α-HL and MspA between the stem side and the vestibule side.[40,41] Figure 1d shows current-voltage curves of α-HL and MspA, respectively. Absolute current values in MspA are higher than those in α-HL at different voltages (i.e. higher slope of I–V curve), which can be attributed to larger and more focused ion current density produced in the constriction zone of MspA due to its higher pore conductance.[42,43]

Characterization of PEO-b-PSS and PEO-b-PVBTMA.—DNA-peptide conjugates have been shown to improve the resolution of nanopore translocation.[24] To create a synthetic analogue to the DNA-peptide systems, diblock polyelectrolytes of poly(styrene sulfonate) (PSS) and poly((vinylbenzyl) trimethyl ammonium) (PVBTMA) were grown from neutral PEO macroinitiators via aqueous reversible addition-fragmentation chain transfer (aRAFT) polymerization to provide PEO-b-PSS and PEO-b-PVBTMA.[36] aRAFT polymerization provides excellent control of diblock size and dispersity, which is crucial for achieving uniform translocation signals through a nanopore, including signal shape, current drop, as well as dwell time. The opposite charge of the diblocks resulted in dramatically different zeta potentials for PEO-b-PSS and PEO-b-PVBTMA. Moreover, both the PEO-b-PSS and PEO-b-PVBTMA maintained a relatively stable value of zeta potentials in both acidic and alkaline conditions as shown in Fig. 2 which indicated that PEO-b-PSS and PEO-b-PVBTMA were tolerant in different nanopore detecting conditions.

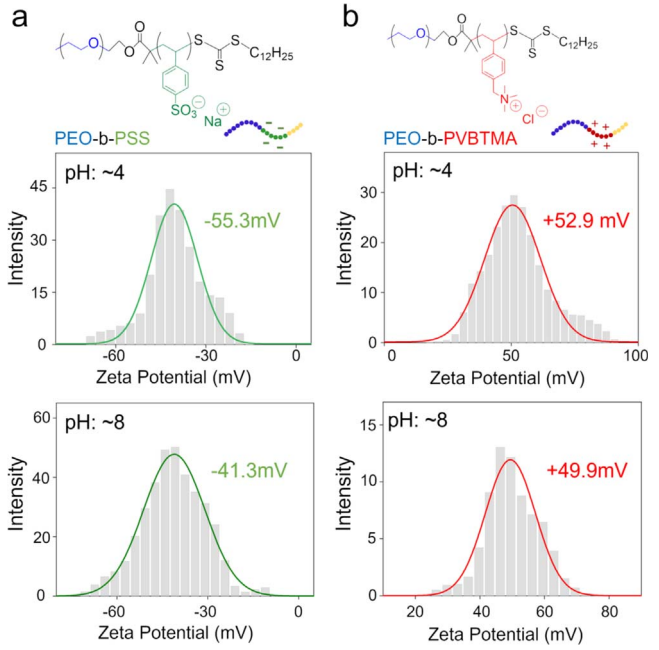

Figure 2. Structures and zeta potentials in acidic and alkaline conditions of PEO-b-PSS (a) and PEO-b-PVBTMA (b).

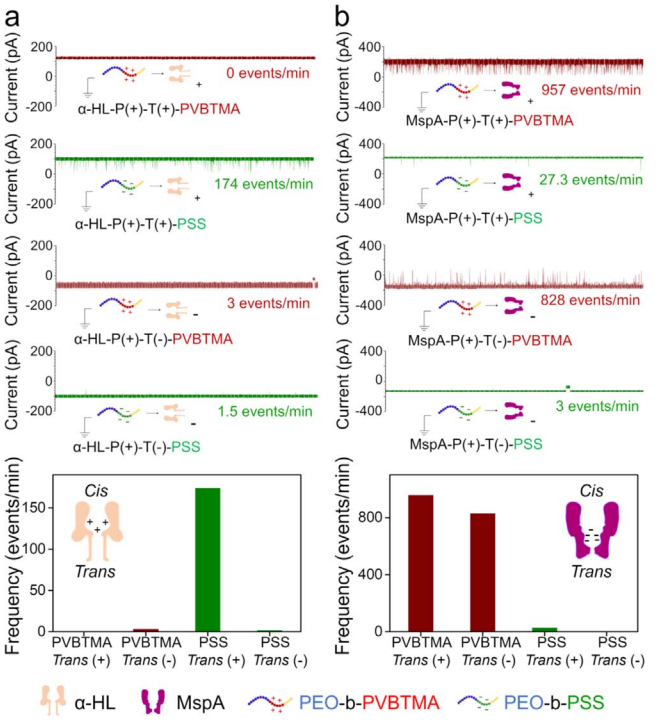

Figure 3. Translocation recordings of PEO-b-PVBTMA and PEO-b-PSS through α-HL and MspA single nanopores in different configurations. (a) Forward α-HL pore P(+) with *trans* chamber held positive T(+) and negative T(−); (b) Forward MspA pore P(+) with *trans* chamber held positive T(+) and negative T(−). Data was collected in 1 M KCl, 10 mM Tris-HCl electrolyte, pH 8.0, with applied voltage held at ±100 mV.

Translocation behaviors in different nanopore configurations.—Analytes entering from different sides of a nanopore-channel could contribute to different translocation recordings.[44] And the applied positive or negative voltage of the *trans* chamber can generate distinct translocation recordings. To investigate the translocation behaviors of PEO-b-PSS and PEO-b-PVBTMA through α-HL and MspA nanopores, we collected translocation recordings in all the possible configurations. When an α-HL mushroom-shaped side or MspA goblet-like was in *the cis* side, it was defined as forwarded pore as P(+). And so, the reverse pore was P(−). The orientation of nanopore insertion can be determined by the absolute value of open-pore current under positive and negative voltages.[38,45] When the voltage applied in the *trans* side was positive, it was defined as T(+), and when the voltage was negative, it was defined as T(−). All the samples entered through the *cis* side, which was grounded. Therefore, for example, α-HL-P(+)-T(+)-PVBTMA indicated PEO-b-PVBTMA translocating through α-HL with a forward pore and positive applied voltage in the *trans* side; MspA-P(-)-T(-)-PSS indicated when PEO-b-PSS translocating through MspA with a reverse pore and negative applied voltage in the *trans* side. In previous studies, neutral blocks PEG have been shown to have high rate of translocation through α-HL.[46] Confinement of PEO electrolytes in inorganic nanoporous particles increases ionic conduction as the pore size decreases with the highest conductivity occurring in pores.[47] Similarly, excellent conductance of neutral PEO blocks was observed in our result as demonstrated by its high capture rate. Meanwhile, the PEO portion of the diblock architecture also lower its fabrication cost.

As indicated in Fig. 3a, in α-HL-P(+)-T(+)-PVBTMA configuration, PEO-b-PVBTMA showed no translocation signals (0 events min^{-1}). PEO-b-PVBTMA is positively charged and the *trans* side of α-HL is applied with positive voltage, which eliminates the translocation driving force. While in α-HL-P(+)-T(-)-PVBTMA configuration, PEO-b-PVBTMA showed low translocation rate of 3 events min^{-1} which could be due to the electrophoretic movement of positively charged PEO-b-PVBTMA to the *trans* side with negative voltage applied. In α-HL-P(+)-T(+)-PSS configuration, a high frequency (174 events min^{-1}) of resistive pulse signals were observed, which can be attributed to the strong driving force between the negatively charged PEO-b-PSS and the *trans* side with positive voltage applied. While in α-HL-P(+)-T(-)-PSS configuration, it showed a low translocation frequency as 1.5 event min^{-1} because of lower electrophoretic driving force compared to α-HL-P(+)-T(+)-PSS configuration. The electrophoretic driving force of PEO-b-PSS comes from the opposite charge between the PEO-b-PSS analyte and the α-HL internal vestibule, as well as the voltage applied in the *trans* side. The difference between α-HL-P(+)-T(+)-PSS configuration and α-HL-P(+)-T(-)-PSS configuration was the voltage applied in the *trans* side. As PEO-b-PSS is negatively charged, it lost partial driving force when the *trans* side was applied with negative voltage. Overall, PEO-b-PVBTMA barely showed any translocation through α-HL pore with forward orientation, with either negative or positive voltage applied in *trans* side, suggesting that for translocation of this analyte was dominated by both the nanopore charge, and the chamber voltage applied.

As shown in Fig. 3b, in MspA-P(+)-T(+)-PVBTMA configuration, even with positively charged PEO-b-PVBTMA, strong negative amino acid constriction inside MspA overwhelmed the resistance from positive *trans* voltage, encouraging a high translocation frequency of 957 events min^{-1} of PEO-b-PVBTMA through MspA. Although a slightly lower translocation frequency (828 events min^{-1}) was observed in the MspA-P(+)-T(-)-PVBTMA configuration, there is no significant difference statistically. This result demonstrates that translocation of the positive PEO-b-PVBTMA is dominated by the negatively charged MspA pore lumen regardless of the trans voltage, which can be attributed to current rectification caused by the geometry of MspA.[43] The MspA-P(+)-T(+)-PSS configuration was expected to get high translocation frequency, but PEO-b-PSS showed a relatively low translocation of 27.3 events min^{-1}, demonstrating the strong influence of MspA electric properties. The MspA-P(+)-T(-)-PSS configuration generated a low translocation frequency of 3 events min^{-1}. Overall, PEO-b-PSS showed low translocation through MspA regardless of whether the *trans* side was applied negative or positive

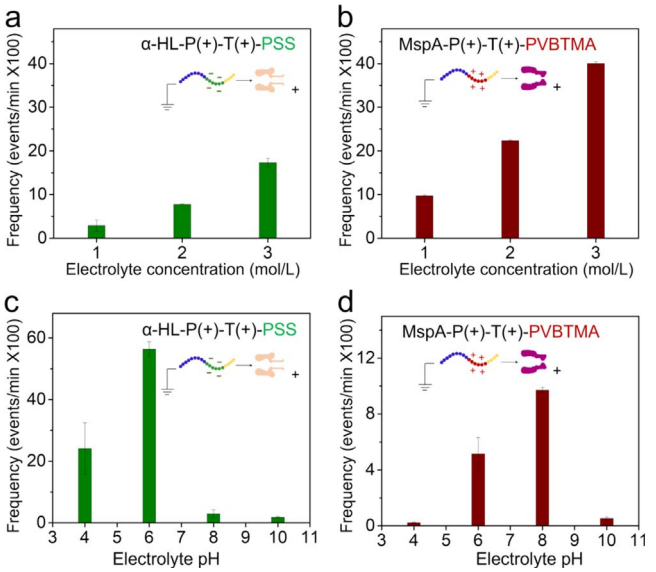

Figure 4. Translocation frequencies of PEO-b-PSS and PEO-b-PVBTMA under α-HL-P(+)-T(+)-PSS and MspA-P(+)-T(+)-PVBTMA configurations, respectively. (a) Translocation of PEO-b-PSS with different concentration (1 M, 2 M, 3 M) of electrolyte solution (KCl, 10 mM Tris-HCl), pH 8.0. (b) Translocation of PEO-b-PVBTMA with different concentration (1 M, 2 M, 3 M) of electrolyte solution (KCl, 10 mM Tris-HCl), pH 8.0. (c) Translocation of PEO-b-PSS with different pH (4.0, 6.0, 8.0, and 10.0) of electrolyte solution (1 M KCl, 10 mM Tris-HCl). (d) Translocation of PEO-b-PVBTMA with different pH (4.0, 6.0, 8.0, and 10.0) of electrolyte solution (1 M KCl, 10 mM Tris-HCl). Data was acquired with the transmembrane potential held at 100 mV.

voltage, proving that the type of nanopore affects translocation behaviors, consistent with the results in α-HL.

Figure S1 (available online at stacks.iop.org/JES/169/057510/mmedia) demonstrated all the configurations when pores were reversed. Almost all the configurations showed less translocation relative to the similar configuration with pores forward. As reported, frequency is smaller for the stem entrance than for the vestibule one, due to a smaller coupling with the electric field and larger activation energy for entry.[48] The different spatial steric hindrance between the bigger vestibule and smaller stem side might cause this result.

Effect of electrolyte concentration and pH on translocation.— In above mentioned results, α-HL-P(+)-T(+)-PSS, MspA-P(+)-T(+)-PVBTMA, and MspA-P(+)-T(-)-PVBTMA configurations all showed high translocation frequencies. We have chosen α-HL-P(+)-T(+)-PSS and MspA-P(+)-T(+)-PVBTMA as representatives for further PEO-b-PSS and PEO-b-PVBTMA translocation studies. First, we investigated the effect of electrolyte concentrations on translocations of PEO-b-PSS and PEO-b-PVBTMA. Figures 4a and 4b show that as the electrolyte concentrations increased from 1 M to 3 M, both PEO-b-PSS and PEO-b-PVBTMA translocation frequency increased. Our results indicate that increasing the electrolyte concentration in the chamber accelerates both PEO-b-PSS and PEO-b-PVBTMA translocation through α-HL and MspA nanopores, respectively. This confirms that electrostatic interactions between analytes and nanopores and ion concentration of the work solution can affect the translocation efficiency.[49] Moreover, high concentration of salt in the work solution can also cause electro-osmotic flow through the nanopore.[50] This finding could be used to optimize next generation biosensing assays to achieve a lower limit of detection.

We also studied the effect of electrolyte pH on translocation. As shown in Fig. 4c, translocation occurred with extremely high frequencies at pH 4.0 and pH 6.0 when PEO-b-PSS was added to the *cis* side. However, when PEO-b-PSS was added to the *cis* compartment in alkaline conditions, current events showed much lower frequencies at pH 8.0 and pH 10.0. As α-HL is a self-assembled heptamer protein that shows globally positively charge with positively and negatively charged residues in its vestibule and β-barrel, respectively. Upon lowering the pH, the β-barrel part becomes less negatively charged, therefore the internal pore surface becomes more positively charged globally, which dramatically increase both capture and threading of the polymer, leading to the increase in PEO-b-PSS translocation in acidic environments.[51] In Fig. 4d, when PEO-b-PVBTMA was added into pH close to the conditions it showed relatively low frequencies at pH 4.0 and pH 8.0. This might also result from the pH of the aqueous environment affecting the net charge of MspA and altering the electrostatic interaction between PVBTMA and the MspA.

Conclusions

DNA molecules are widely used as probes for sensing via nanopore translocation since the electrophoretic force acting on the charged DNA backbone provides a driving force for analytes' translocation through nanopores. DNA-neutral peptide conjugates have been shown to be even more beneficial to this process and increase the resolution of the nanopore signal. To improve on these DNA-peptide systems, we explored synthetic charged-neutral polyelectrolyte analogues. Synthetic polyelectrolytes have the benefit of being able to be positively or negatively charged, which expands the design space for nanopore sensing probes. In this study, we investigated the translocation behaviors of two oppositely charged diblock polyelectrolytes through two commonly used biological nanopores: α-HL and MspA. The translocation recordings presented in this paper proved efficient PEO-b-PSS translocations through α-HL and PEO-b-PVBTMA translocations through MspA, that validate the potential of synthetic diblock polyelectrolytes as probes to enable nanopore detection for uncharged or lower charged analytes. Specifically, uncharged, or lower charged analytes such as peptides and proteins are lack of driving force to translocate through nanopores. When these analytes are conjugated with highly charged polyelectrolytes, the polyelectrolyte can "drag" the analyte through the nanopore. Comparing to low frequency translocation of bare analytes, higher translocation frequency of polyelectrolytes conjugated analytes enable detection with higher sensitivity. In contrast to DNA systems, synthetic polyelectrolytes can be positively or negatively charged, can bear a variety of functional groups, and can be configured in a number of structural arrangements. This vastly expands the number of potential probe molecules and pore proteins available for use in nanopore translocation. Furthermore, synthetic polyelectrolytes can have a wide range of sizes and structures, while natural DNA has either flexible single-stranded structures or helical double-stranded structures. Based on our results, we believe synthetic diblock polyelectrolytes are promising candidates for probes within nanopore sensing.

Acknowledgments

C. Liu acknowledges support from the Biomedical Engineering Program and Department of Chemical Engineering, University of South Carolina; the National Institute of Allergy and Infectious Diseases (NIAID) award K22AI136686; the South Carolina IDeA Networks of Biomedical Research Excellence Developmental Research Project by the National Institute of General Medical Sciences (NIGMS) award P20GM103499, and the National Science Foundation (NSF) CAREER Award 2047503.

Notes

The authors declare no competing financial interest.

ORCID

Xiaoqin Wang https://orcid.org/0000-0003-3884-9635
Kaden C. Stevens https://orcid.org/0000-0002-5853-8765
Alexander E. Marras https://orcid.org/0000-0001-8972-9532

Gelareh Rezvan https://orcid.org/0000-0002-5203-6801
Xiaojun Wei https://orcid.org/0000-0002-6229-6228
Nader Taheri-Qazvini https://orcid.org/0000-0003-2114-7338
Chang Liu https://orcid.org/0000-0001-8097-9631

References

1. K. Lee, K. B. Park, H. J. Kim, J. S. Yu, H. Chae, H. M. Kim, and K. B. Kim, *Adv. Mater.*, **30**, 1704680 (2018).
2. A. Oukhaled, L. Bacri, M. Pastoriza-Gallego, J.-M. Betton, and J. Pelta, *ACS Chem. Biol.*, **7**, 1935 (2012).
3. J. W. Robertson and J. E. Reiner, *Proteomics*, **18**, 1800026 (2018).
4. S. Xie, A. W. Leung, Z. Zheng, D. Zhang, C. Xiao, R. Luo, M. Luo, and S. Zhang, *The Innovation*, **2**, 100153 (2021).
5. J. Wilson, L. Sloman, Z. He, and A. Aksimentiev, *Adv. Funct. Mater.*, **26**, 4830 (2016).
6. J. J. Kasianowicz, J. W. Robertson, E. R. Chan, J. E. Reiner, and V. M. Stanford, *Annu. Rev. Anal. Chem.*, **1**, 737 (2008).
7. Z. Zhang, X. Wang, X. Wei, S. W. Zheng, B. J. Lenhart, P. Xu, J. Li, J. Pan, H. Albrecht, and C. Liu, *Biosens. Bioelectron.*, **181**, 113134 (2021).
8. S. Howorka and Z. Siwy, *Chem. Soc. Rev.*, **38**, 2360 (2009).
9. Z. L. Hu, M. Z. Huo, Y. L. Ying, and Y. T. Long, *Angew. Chem.*, **133**, 14862 (2021).
10. X. Wei, D. Ma, Z. Zhang, L. Y. Wang, J. L. Gray, L. Zhang, T. Zhu, X. Wang, B. J. Lenhart, and Y. Yin, *ACS Sens.*, **5**, 1707 (2020).
11. B. Lenhart, X. Wei, B. Watson, X. Wang, Z. Zhang, C. Z. Li, M. Moss, and C. Liu, *Sensors Actuators B*, **338**, 129863 (2021).
12. G. F. Schneider and C. Dekker, *Nat. Biotechnol.*, **30**, 326 (2012).
13. P. N. Pratanwanich, F. Yao, Y. Chen, C. W. Koh, Y. K. Wan, C. Hendra, P. Poon, Y. T. Goh, P. M. Yap, and J. Y. Chooi, *Nat. Biotechnol.*, **39**, 1394 (2021).
14. M. Wanunu, *Phys. Life Rev.*, **9**, 125 (2012).
15. S. J. Heerema and C. Dekker, *Nat. Nanotechnol.*, **11**, 127 (2016).
16. L. Song, M. R. Hobaugh, C. Shustak, S. Cheley, H. Bayley, and J. E. Gouaux, *Science*, **274**, 1859 (1996).
17. G. A. Bohach and I. S. Snyder, *J. Bacteriol.*, **164**, 1071 (1985).
18. J. R. Thompson, B. Cronin, H. Bayley, and M. I. Wallace, *Biophys. J.*, **101**, 2679 (2011).
19. M. Krause, A. M. Niazi, K. Labun, Y. N. T. Cleuren, F. S. Müller, and E. Valen, *RNA*, **25**, 1229 (2019).
20. T. Zhao, H.-S. Zhang, H. Tang, and J.-H. Jiang, *Talanta*, **175**, 121 (2017).
21. R. R. Zascavage, K. Thorson, and J. V. Planz, *Electrophoresis*, **40**, 272 (2019).
22. M. J. N. Sampad, H. Zhang, T. D. Yuzvinsky, M. A. Stott, A. R. Hawkins, and H. Schmidt, *Biosens. Bioelectron.*, **194**, 113588 (2021).
23. L. Liu and H. C. Wu, *Angew. Chem. Int. Ed.*, **55**, 15216 (2016).
24. S. Biswas, W. Song, C. Borges, S. Lindsay, and P. Zhang, *ACS nano*, **9**, 9652 (2015).
25. N. Liu, Z. Yang, X. Lou, B. Wei, J. Zhang, P. Gao, R. Hou, and F. Xia, *Anal. Chem.*, **87**, 4037 (2015).
26. B. Guo, Y. Sheng, K. Zhou, Q. Liu, L. Liu, and H. C. Wu, *Angew. Chem.*, **130**, 3664 (2018).
27. L. Liu, Y. You, K. Zhou, B. Guo, Z. Cao, Y. Zhao, and H. C. Wu, *Angew. Chem.*, **131**, 15071 (2019).
28. T. Z. Butler, M. Pavlenok, I. M. Derrington, M. Niederweis, and J. H. Gundlach, *Proc. Natl Acad. Sci.*, **105**, 20647 (2008).
29. M. Niederweis, S. Ehrt, C. Heinz, U. KloÈcker, S. Karosi, K. M. Swiderek, L. W. Riley, and R. Benz, *Mol. Microbiol.*, **33**, 933 (1999).
30. Y. Wang, X. Guan, S. Zhang, Y. Liu, S. Wang, P. Fan, X. Du, S. Yan, P. Zhang, and H.-Y. Chen, *Nat. Commun.*, **12**, 1 (2021).
31. S. Yan, J. Zhang, Y. Wang, W. Guo, S. Zhang, Y. Liu, J. Cao, Y. Wang, L. Wang, and F. Ma, *Nano Lett.*, **21**, 6703 (2021).
32. A. V. Dobrynin and M. Rubinstein, *Prog. Polym. Sci.*, **30**, 1049 (2005).
33. X. Zhang, Y. Wang, B. L. Fricke, and L.-Q. Gu, *ACS nano*, **8**, 3444 (2014).
34. K. Shoji, R. Kawano, and R. J. White, *ACS nano*, **13**, 2606 (2019).
35. T. J. Morin, T. Shropshire, X. Liu, K. Briggs, C. Huynh, V. Tabard-Cossa, H. Wang, and W. B. Dunbar, *PLoS One*, **11**, e0154426 (2016).
36. J. M. Ting, H. Wu, A. Herzog-Arbeitman, S. Srivastava, and M. V. Tirrell, *ACS Macro Letters*, **7**, 726 (2018).
37. C. Yang, L. Liu, T. Zeng, D. Yang, Z. Yao, Y. Zhao, and H.-C. Wu, *Anal. Chem.*, **85**, 7302 (2013).
38. X. Wei, Z. Zhang, X. Wang, B. Lenhart, R. Gambarini, J. Gray, and C. Liu, *Nanotechnology and Precision Engineering*, **3**, 2 (2020).
39. X. Wei, Q. Wang, and C. Liu, *Proteomics*, **22**, 2100058 (2022).
40. S. Tseng, S.-C. Lin, C.-Y. Lin, and J.-P. Hsu, *The Journal of Physical Chemistry C*, **120**, 25620 (2016).
41. P. Y. Apel, I. V. Blonskaya, O. L. Orelovitch, P. Ramirez, and B. A. Sartowska, *Nanotechnology*, **22**, 175302 (2011).
42. I. M. Derrington, T. Z. Butler, M. D. Collins, E. Manrao, M. Pavlenok, M. Niederweis, and J. H. Gundlach, *Proceedings of the National Academy of Sciences,*, **107**, 16060 (2010).
43. W. Zhou, H. Qiu, Y. Guo, and W. Guo, *J. Phys. Chem. B*, **124**, 1611 (2020).
44. N. A. Bell, K. Chen, S. Ghosal, M. Ricci, and U. F. Keyser, *Nat. Commun.*, **8**, 1 (2017).
45. X. Wei, D. Ma, L. Jing, L. Y. Wang, X. Wang, Z. Zhang, B. J. Lenhart, Y. Yin, Q. Wang, and C. Liu, *J. Mater. Chem. B*, **8**, 6792 (2020).
46. D. C. Machado, J. J. Júnior, M. C. Melo, A. M. Silva, A. Fontes, and C. G. Rodrigues, *RSC Adv.*, **6**, 56647 (2016).
47. S. Vorrey and D. Teeters, *Electrochim. Acta*, **48**, 2137 (2003).
48. G. Gibrat, M. Pastoriza-Gallego, B. Thiebot, M.-F. Breton, L. Auvray, and J. Pelta, *J. Phys. Chem. B*, **112**, 14687 (2008).
49. C. H. Wang, M. B. Luo, X. Xu, C. Wang, and L. Z. Sun, *Eur. Polym. J.*, **121**, 109332 (2019).
50. X. Chen, Y. Zhang, G. Mohammadi Roozbahani, and X. Guan, *ACS applied bio materials*, **2**, 504 (2018).
51. E. L. Bonome, F. Cecconi, and M. Chinappi, *Microfluid. Nanofluid.*, **21**, 1 (2017).